CrossMark

Development process of muzzle flows including a gun-launched missile

Zhuo Changfei, Feng Feng *, Wu Xiaosong

School of Mechanical Engineering, Nanjing University of Science and Technology, Nanjing 210094, China

Abstract Numerical investigations on the launch process of a gun-launched missile from the muzzle of a cannon to the free-flight stage have been performed in this paper. The dynamic overlapped grids approach are applied to dealing with the problems of a moving gun-launched missile. The high-resolution upwind scheme (AUSMPW +) and the detailed reaction kinetics model are adopted to solve the chemical non-equilibrium Euler equations for dynamic grids. The development process and flow field structure of muzzle flows including a gun-launched missile are discussed in detail. This present numerical study confirms that complicated transient phenomena exist in the shortly launching stages when the gun-launched missile moves from the muzzle of a cannon to the free-flight stage. The propellant gas flows, the initial environmental ambient air flows and the moving missile mutually couple and interact. A complete structure of flow field is formed at the launching stages, including the blast wave, base shock, reflected shock, incident shock, shear layer, primary vortex ring and triple point.
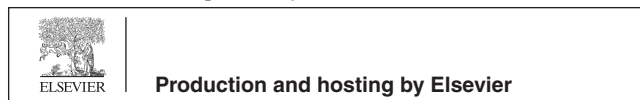
1. Introduction

The gun-launched missile[1–3] is a special missile launched by tank or cannon. It can obtain a high initial velocity by cannon and then use rocket engine to further accelerate. Compared with the general projectile and missile, the gun-launched missile has many advantages such as reducing launch cost, improving hitting accuracy and extending firing range, which is a rapid developing guided weapon in recent years.

* Corresponding author. Tel.: + 86 25 84303185.
E-mail address: nust203@aliyun.cn (F. Feng).
Peer review under responsibility of Editorial Committee of CJA.

The muzzle flows induced by a general projectile moving from the muzzle of a cannon to the free-flight stage are a complex blast flow field, which have the characteristics of unsteady flow, strong shock discontinuity and severe chemical reactions. Several wave phenomena are defined, such as blast wave, incident shock, reflected shock, and Mach disk. It is important to study the mechanism of muzzle flows to improve or increase the efficiency of weapon. There have been many investigations about muzzle flow[4–10] in the past years. For instance, Cler[8] adopted the Fluent 6.1 solvers and discontinuous Galerkin (DG) solver to simulate the muzzle flows without a projectile. Shock waves' dynamics process of the muzzle flows was numerically visualized in detail through special treatment on the moving cylinder projectile in the shock wave tube by Jiang and Takayama.[9] In the previous numerical simulation studies of muzzle flows, the majority of researchers did not consider the muzzle flows affected by the high-speed moving projectile. In

the calculation process, it is needed not only to deal with the complex shock discontinuity, but also to consider computational grid changes due to the high-speed moving projectile, which led to complicated calculation process. At the same time, they did not consider the real propellant gas and just assumed that the real propellant gas in the cannon tube to be air, which was the same as external ambient air. They also ignored the chemical reactions between the real propellant gas and the external air. Although the calculation was simplified, the accuracy was insufficient and could only estimate the flow field. In order to accurately study the muzzle flows induced by a supersonic projectile moving from the muzzle of a cannon to the free-flight stage, the muzzle flows affected by the real high-speed moving projectile and the propellant gas must be considered.

However, according to the published literature, a study of the muzzle flows including a gun-launched missile is not nearly performed. After all, it is difficult to study this process and obtain data by experimental methods since the gun-launched missile moves from the muzzle to the surroundings in any extremely short time. On the other hand, due to the rising cost of experimental measurements together with limited experimental facilities and testing technology, it is of great significance to establish a reasonable and accurate calculation method for muzzle flows including a gun-launched missile.

For a moving body flow problem, the computational grids must move with the body. The most straightforward approach is to deform the computational grid locally using a spring-analogy type algorithm to follow the motion of the moving body.[11] This approach is very efficient because it does not require solution interpolation, but a disadvantage of the approach is that the grid integrity can be destroyed by large motions or shear-type of boundary motions. The dynamic overlapped grids approach seems to be the state-of-the-art in handling moving boundary problems and has been used successfully for a variety of applications.[12–14] The dynamic grids are generated first near the moving body and the static grids are generated for background overlapped with the dynamic grids. With the motion of moving body, the dynamic grids move with the moving body on the static background grids. It is demonstrated that this approach dealing with moving body is accurate and efficient.

The present study aims at establishing a reasonable and accurate calculation method for muzzle flows including a gun-launched missile in conjunction with the chemical reactions. The dynamic overlapped grids' approach are applied to dealing with the problems of a gun-launched missile. The high-resolution upwind scheme (AUSMPW+) and the detailed reaction kinetics model are adopted to solve the ALE (Arbitrary Lagrangian Eulerian) Euler equations with chemical reactions. A special case is chosen for the validation of the numerical algorithms. After checking the accuracy of the numerical algorithms, the case of the muzzle flows including a gun-launched missile is simulated. Using the numerical results, the development process of muzzle flows including a gun-launched missile is visualized numerically and discussed in detail.

2. Mathematical method

2.1. Governing equations

Assuming that the muzzle flows in the present study are two-dimensional axisymmetric during the short time duration while the gun-launched missile moves from the muzzle of a cannon to the free-flight stage, the time-dependent ALE Euler equations with chemical non-equilibrium are expressed in the integral form as

$$\frac{\partial}{\partial t} \int \int_V \boldsymbol{Q}dV + \oint_S (\boldsymbol{F}(\boldsymbol{Q})n_x + \boldsymbol{G}(\boldsymbol{Q})n_y)\mathrm{d}S$$
$$= \int \int_V (\boldsymbol{H}_1 + \boldsymbol{H}_2)\mathrm{d}V \tag{1}$$

where S is the surface surrounding the control volume V, $\boldsymbol{n} = n_x\boldsymbol{i} + n_y\boldsymbol{j}$ the out-going unit normal of S, $\boldsymbol{Q}$ the vector of the conservative variables, $\boldsymbol{H}_1$ the vector of source term caused by chemical reactions, and $\boldsymbol{H}_2$ the vector of source term caused by axial symmetry, $\boldsymbol{F}$, $\boldsymbol{G}$ are the vectors of the convective flux. Here, $\boldsymbol{Q}$, $\boldsymbol{F}$, $\boldsymbol{G}$, $\boldsymbol{H}_1$, $\boldsymbol{H}_2$ are given by

$$\begin{cases} \boldsymbol{Q} = [\rho \quad \rho u \quad \rho v \quad E \quad \rho f_i]^{\mathrm{T}} \\ \boldsymbol{F} = [\rho(u-u_w) \quad \rho u(u-u_w)+p \quad \rho v(u-u_w) \quad (E+p)(u-u_w) \quad \rho f_i(u-u_w)]^{\mathrm{T}} \\ \boldsymbol{G} = [\rho(v-v_w) \quad \rho u(v-v_w) \quad \rho v(v-v_w)+p \quad (E+p)(v-v_w) \quad \rho f_i(v-v_w)]^{\mathrm{T}} \\ \boldsymbol{H}_1 = [0 \quad 0 \quad 0 \quad 0 \quad \omega_i]^{\mathrm{T}} \\ \boldsymbol{H}_2 = -\frac{v}{y}[\rho \quad \rho u \quad \rho v \quad E+p \quad \rho f_i]^{\mathrm{T}} \end{cases}$$

$$\tag{2}$$

where ρ is the density, p the pressure, and f_i the mass fraction of species i; u, v are the velocity components of fluids, u_w, v_w the moving velocity components of the surface S. The subscripts $i = 1, 2, \cdots, N-1$, where N is the total number of species. ω_i given by the chemical reaction kinetic model is the mass production rate of species i:

$$\omega_i = M_i \sum_{j=1}^{N} (\beta_{ij} - \alpha_{ij})(R_{fj} - R_{bj}) \tag{3}$$

where M_i is the molar mass of species i; R_{fj} and R_{bf} are the positive reaction rate and the reverse reaction rate of elementary reaction, respectively, α_{ij} and β_{ij} the stoichiometric coefficients of species i in the jth elementary reaction; N is the total number of elementary reaction.

The total energy E is defined as

$$E = \rho h - p + \frac{1}{2}\rho(u^2 + v^2) \tag{4}$$

where h is the specific enthalpy of the gas mixture.

2.2. Numerical methods

In order to improve the accuracy of spatial discretization, we should reconstruct the primitive variables before computing the convection flux quantities of the governing equation using upwind scheme.

In the computational domain of structured grid, the non-oscillatory and non-free-parameter dissipation (NND) scheme[15] is used. In the computational domain of unstructured grid, the reconstruction method in Ref. [16] presented by Barth and Jespersen is used in this study.

Convection flux quantities are computed by using the AUSMPW+ scheme[17] with reconstructed state primitive variables on both sides of a face, after completing the reconstruction in the cell interface. AUSMPW+ scheme has higher resolution in capturing oblique shocks than any other AUSM-type scheme. Furthermore, the AUSMPW+ scheme is more efficient to implement than AUSMPW while maintaining the same level of the robustness and accuracy.

2.3. Chemical reaction kinetic model and numerical stiffness

One of the keys to determine the success of chemical non-equilibrium flow simulation is the chemical reaction kinetic model. In the current work, the chemical reaction kinetic model of carbon monoxide oxidation involves 8 species (CO, H_2, O_2, CO_2, H_2O, H, OH, O), 1 inert specie (N_2) and 12 elementally reactions steps,[18] which are shown in Table 1.

In the chemical reaction flow filed, the characteristic chemical time τ_{chem} is much smaller than the characteristic flow time τ_{flow}, meaning the Damkohler number ($Da = \tau_{flow}/\tau_{chem}$) is much larger than 1, and then the stiff problem is formed. The time-operator splitting algorithm[19] is used to deal with the stiff problem.

3. Principle of dynamic overlapped grid and computational model

Dynamic overlapped grids approach mainly includes two parts. The first one is that the computational domain is divided into multiple overlapped subdomains, and the inside and outside boundaries of the overlapped subdomains are given. The second one is that the flow information is exchanged among the subdomains. This exchange process uses the fourth-order interpolation scheme[20] that the interpolation accuracy of this method is sufficient. In an entire time step "dt" (from t^n to t^{n+1}), the flow parts and chemical reaction parts are needed to solve. Once the calculations in this time step is completed, the flow information will be exchanged among the overlapped subdomain, and the location of dynamic overlapped subdomain will also be updated. In the present work, two sets of grid systems are established to compute the muzzle flows: the static background grid describing the cannon tube and the surroundings near the cannon, and the dynamic grid around the missile describes its high-speed movement. In order to adapt to the complex shape of the head of the missile, an unstructured grid is used to describe the head of missile. The overall computational domain of muzzle flows including a gun-launched missile is shown in Fig. 1. The diameters of the missile and the cannon tube are both 155 mm, the length of cannon tube is

6 m, the right boundary of the computational domain is 5 m downstream from the cannon, and the distance between the top boundary of the computational domain and the symmetrical axis is 3 m. According to the symmetry, only half of the physical model needs to be calculated.

For this paper, to reduce the computational time, instead of considering the motion of gun-launched missile in the cannon tube, the calculation starts when the bottom of gun-launched missile leaves the muzzle of a cannon. The gun-launched missile moves outside the cannon according to Newton's second law of motion. The time when the bottom of gun-launched missile leaves the muzzle of a cannon is defined as $t = 0$ s, and the relative position between the gun-launched missile and the cannon at $t = 0$ s is shown in Fig. 2. According to the law of interior ballistics of the cannon, the velocity of the propellant gas in the cannon tube linearly varies with distance. The velocity of the propellant gas at the bottom of cannon is zero, while the velocity of propellant gas in the muzzle of a cannon is $V_0 = 900$ m/s, which is equal to the initial velocity (launching velocity) of gun-launched missile when the gun-launched missile leaves the muzzle of a cannon. The temperature of the propellant gas is 2000 K and the pressure is $p_0 = 60$ MPa. The total temperature and total pressure of the rocket gas injected from the bottom of missile are 2200 K and 10 MPa, respectively. The composition and mass fraction of the propellant gas and rocket gas are shown in Table 2. Besides the rocket gas boundary, there are two other boundary conditions, the solid and free boundaries. The former includes static solid boundary (i.e., the inner and outer surfaces of the cannon tube) and the moving solid boundary (i.e., surfaces of the missile). Both of these are assumed as slip boundary, i.e., the normal velocity component of the static solid boundary is zero, while that of the moving solid is equal to the component of the moving missile. Since the latter (free boundary) is only affected by the interior, its interface flux is always equal to the flux of the cell-centered values. The axially symmetric boundary is the same as a static solid boundary because the solid boundary is a slip boundary.

At the initial time $t = 0$ s, the ambient air conditions near the cannon are at $p_a = 101325$ Pa and $T_a = 293$ K. The

Table 1 Chemical reaction kinetic model of $CO–H_2–O_2$ system.

Detailed reaction	A	b	E
$H + O_2 \leftrightarrow OH + O$	1.2×10^{17}	-0.91	69.1
$H_2 + O \leftrightarrow OH + H$	1.5×10^7	2.0	31.6
$O + H + M \leftrightarrow OH + M$	1.0×10^{16}	0	0
$O + O + M \leftrightarrow O_2 + M$	1.0×10^{17}	-1.0	0
$H + H + M \leftrightarrow H_2 + M$	9.7×10^{16}	-0.6	0
$H_2O + M \leftrightarrow H + OH + M$	1.6×10^{17}	0	478.0
$O + H_2O \leftrightarrow OH + OH$	1.5×10^{10}	1.14	72.2
$OH + H_2 \leftrightarrow H_2O + H$	1.0×10^8	1.6	13.8
$H_2 + O_2 \leftrightarrow OH + OH$	7.94×10^{14}	0	187.0
$CO + OH \leftrightarrow CO_2 + H$	4.4×10^6	1.5	-3.1
$CO + O + M \leftrightarrow CO_2 + M$	5.3×10^{13}	0	-19.0
$CO + O_2 \leftrightarrow CO_2 + O$	2.5×10^{12}	0	200.0

Notes: Arrhenius form is $K_f = AT^b \exp(-E_0/(R_0 T))$, b the temperature index, E_0 the activation energy, R_0 the specific gas constant, the unit of factor A is $(cm^3/mol)^{n-1} \cdot s^{-1}$, where n is the chemical reaction progression; and M the third body collision.
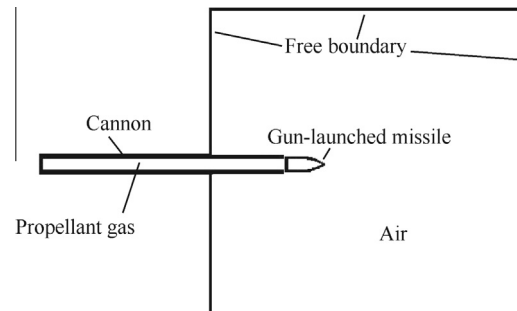
Fig. 1 Schematic of overall computational domain.

Fig. 2 Relative position between missile and cannon at $t = 0$ s.

Table 2 Composition and mass fraction of propellant gas and rocket gas.

Gas	CO	H_2	CO_2	H_2O	N_2
Propellant	0.5138	0.0157	0.2153	0.1293	0.1259
Rocket	0.3402	0.0241	0.3228	0.1627	0.1502

composition and mass fraction of air are N_2-0.77 and O_2-0.23, respectively.

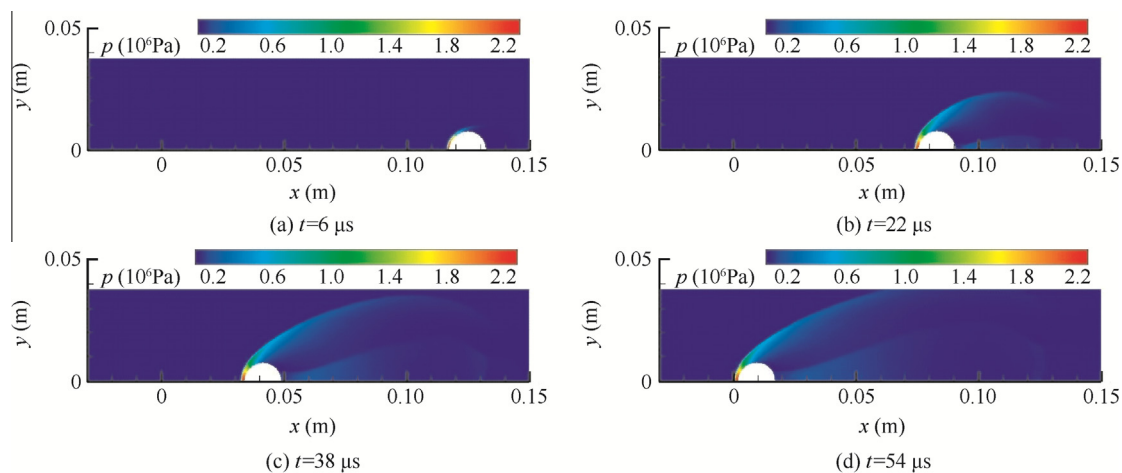## 4. Validating numerical algorithms

The case for validating the dynamic overlapped grids approach and numerical solutions of chemical non-equilibrium flows is the oblique detonation combustion flows induced by hypervelocity sphere in a combustible gas, which is a moving boundary problem of a sphere traveling at $V = 2605$ m/s through a stationary H_2/Air mixture gas (Case A). This case can be simplified to a two-dimensional axisymmetric model. Its computational domain is shown in Fig. 3 ($L_1 = 0.18$ m, $L_2 = 0.04$ m, $L_3 = 0.02$ m, $L_4 = 0.04$ m). The unstructured grid domain around the sphere can move on the stationary background structured grid domain, and the stationary
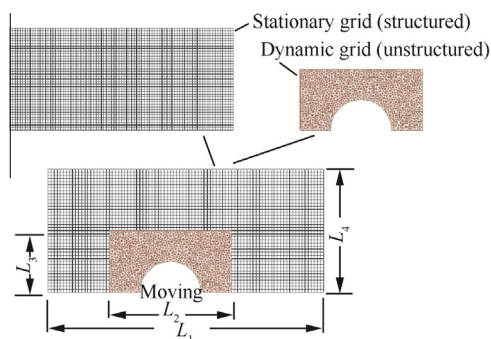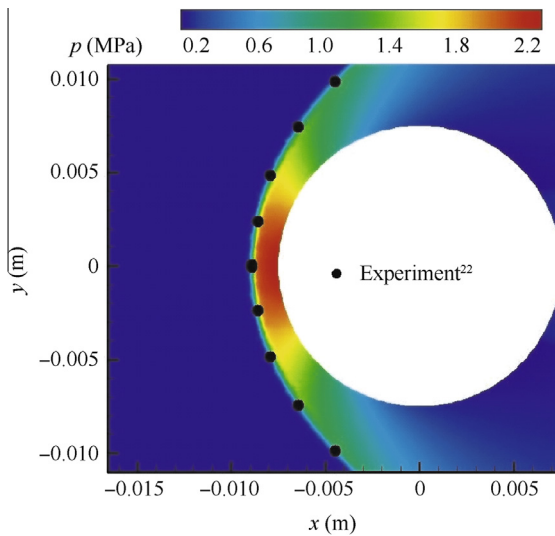
background grid overlapped with dynamic unstructured grid is not involved in the calculation and display (Fig. 3 is only a schematic diagram and the computational domain of the actual calculation is larger and the grid is finer). The unstructured grid domain consists of triangular cells, with node number of 24929 and cell number of 74125. The structured grid domain consists of rectangle cells that the scale of cell is 0.15 mm × 0.15 mm. The time step dt solving governing equations is 1.0×10^{-8} s.

After the initial transients, the flow field around the moving sphere should settle down and become "steady" with respect to the sphere. A major feature of this flow field is an oblique detonation wave in front of the moving sphere. For comparison purpose, this simulation is also run in the steady mode (Case B). The detailed conditions in Case A are as follows: the velocity of the moving sphere is 2605 m/s and the radius of sphere is $R = 0.0075$ m. The H_2/Air mixture gas has a mixture ratio of $2H_2 + O_2 + 3.76N_2$, a velocity of $V_\infty = 0$ m/s, a pressure of $p_\infty = 46626$ Pa and a temperature of $T_\infty = 286.6$ K. The detailed conditions in Case B are as follows: the stationary sphere is fixed on a location in the stationary grid. The H_2/Air mixture gas has a mixture ratio of $2H_2 + O_2 + 3.76N_2$, a velocity of $V_\infty = 2605$ m/s, a pressure of $p_\infty = 46,626$ Pa and a temperature of $T_\infty = 286.6$ K. In the current case, the chemical reaction kinetic model of hydrogen oxidation mechanism with 6 species (H_2, O_2, H_2O, H, OH, O), 1 inert specie (N_2) and 8 elemental reactions[21] is used.

For the moving body simulation, a sequence of pressure contours at the corresponding times is shown in Fig. 4. Note that a bow shock is generated from the wall when the sphere starts to move. Finally the bow shock remains at a fixed location relative to the sphere. The pressure contours from both the moving body simulation (Case A) and the steady state simulation (Case B) are compared in Fig. 5, which also show the comparison with the experimental data of Lehr.[22] In addition, as can be seen in Figs. 6 and 7, the present computational results along the stagnation streamline agree very well with those in Refs.[23,24]. In a word, this case indicates that the implementation of dynamic overlapped grids is successful and the numerical method for solving chemical non-equilibrium flows is also accurate and reliable.

Fig. 3 Schematic of computational domain of validating case.

(a) $t=6$ μs

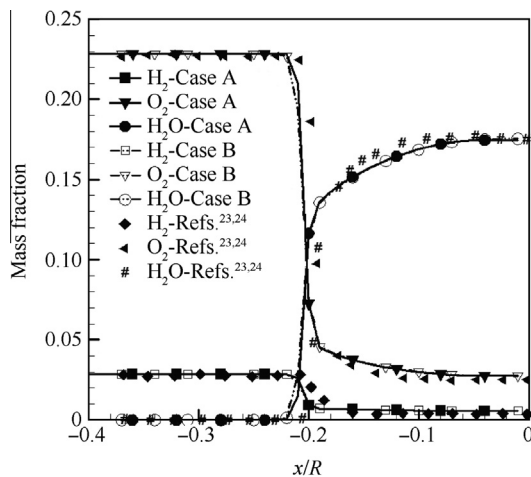(b) $t=22$ μs

(c) $t=38$ μs

(d) $t=54$ μs

Fig. 4 Computed pressure contours at different times.

Fig. 5 Comparison between computed front of detonation wave and experimental reference (upper($y > 0$): Case A; lower($y < 0$): Case B).
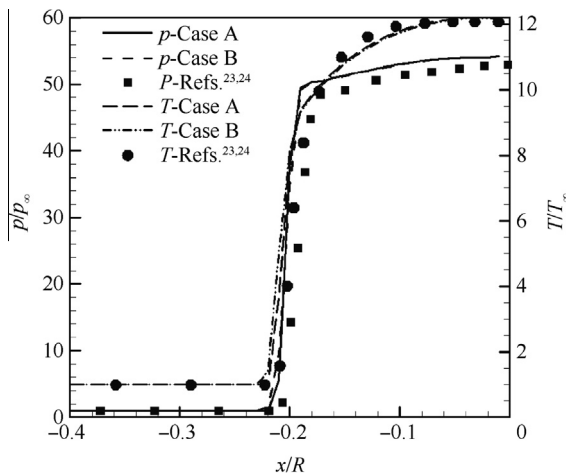
Fig. 6 Distribution of pressure and temperature along stagnation streamline.

Fig. 7 Distribution of mass fraction along stagnation streamline.

5. Numerical results and discussion

5.1. Development process of muzzle flows with gun-launched missile

After gun-launched missile leaves the muzzle of the cannon, the propellant gas with high temperature and high pressure in the cannon tube is suddenly released and rushes out. Simultaneously, the propellant gas flows, the initial environmental ambient air flows, and the moving missile mutually couple and interact. As can be seen in Table 2, the composition and mass fraction of propellant gas, rocket gas and the external air are different, so the mass fraction of H_2 is chosen as a validation that reflects the distribution of propellant gas. The numerical results are presented in a time sequence in Figs. 8–12. Although only the upper half of the physical model is calculated, for better observation, the numerical results of the overall physical model are shown according to the symmetry.

Fig. 8 shows the flow field at $t = 0.5$ ms. When the gun-launched missile is just released from the muzzle of cannon, the propellant gas quickly propagates into the external ambient air and starts to expand and accelerate, leading to a decrease of temperature and an increase of Mach number. The base shock is generated because the velocity of the accelerating propellant gas is much greater than the moving velocity of gun-launched missile. At the same time, the moving velocity of missile relative to the ambient air in external environment is supersonic, resulting in the generation and gradual stability of the bow shock at the head of the missile. However, because the temperature of the bow shock is much lower than that of the propellant gas, the bow shock cannot be clearly found in temperature contours and Mach number contours. In addition, due to the obstruction of both the ambient air in external environment and the gun-launched missile, the blast wave driven by the propellant gas mainly propagates along the radial direction with an annulus-like shape, and the incident shock and Mach cone that gradually develops into Mach disk is generated. There exists a high-temperature zone near the contact surface (between the propellant gas and the external air), which results from the secondary combustion of the CO/H_2 in the propellant gas with the O_2 in the external air.

A typical jet flow structure is observed in Fig. 9 at $t = 1.5$ ms. The bottom of the gun-launched missile moves through the Mach disk, and the base shock disappears as the gas flow behind the Mach disk is in subsonic zone. Meantime, a complete structure of flow field is formed, including the blast wave, base shock, reflected shock, incident shock, shear layer, primary vortex ring and triple point. As can be seen from the distribution of the mass fraction of H_2, the rocket gas containing H_2 has injected from the bottom of gun-launched missile and interacts with the propellant gas.

According to Fig. 10, at $t = 2.5$ ms, with the propagation of the blast wave, the blast wave goes into a decay period, and the axial velocity of the propagation of the blast wave rapidly decreases so that it is less than the moving velocity of gun-launched missile. Then the gun-launched missile will move through the blast wave. In addition, it is also observed that the high-temperature zone near the contact surface disappears, indicating that the degree of the secondary combustion near the contact surface weakens gradually. The reason for the
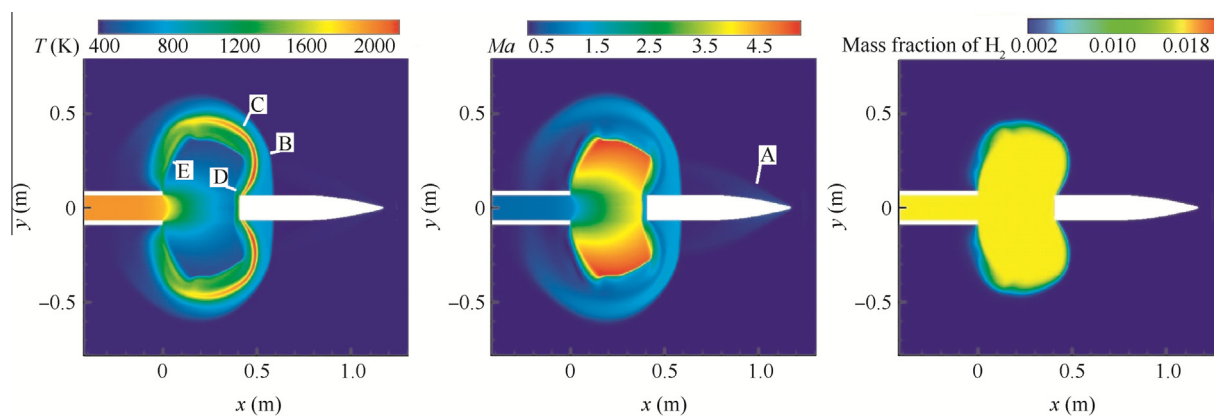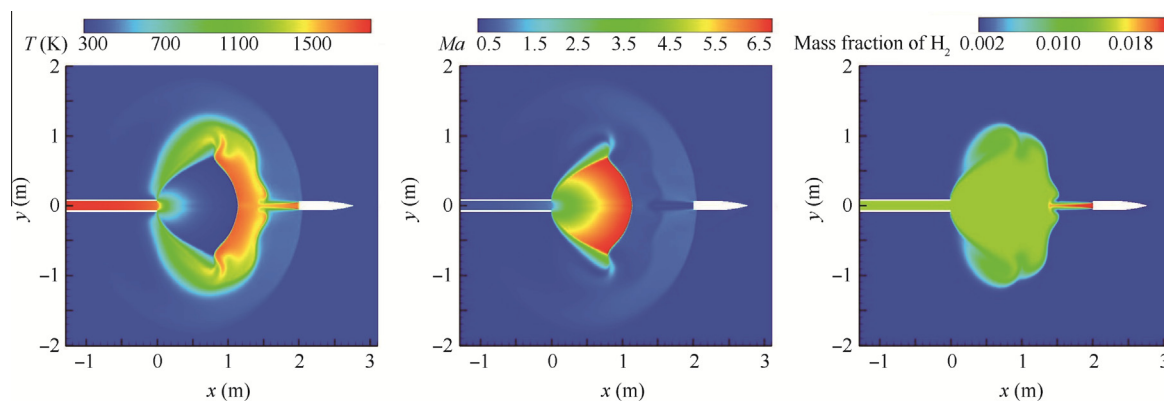
Notes: A—Bow shock; B—Blast wave; C—Contact surface between propellant gas and air; D—Base shock; E—Incident shock

Fig. 8 Contours of temperature, Mach number and mass fraction of H_2 at t = 0.5 ms.
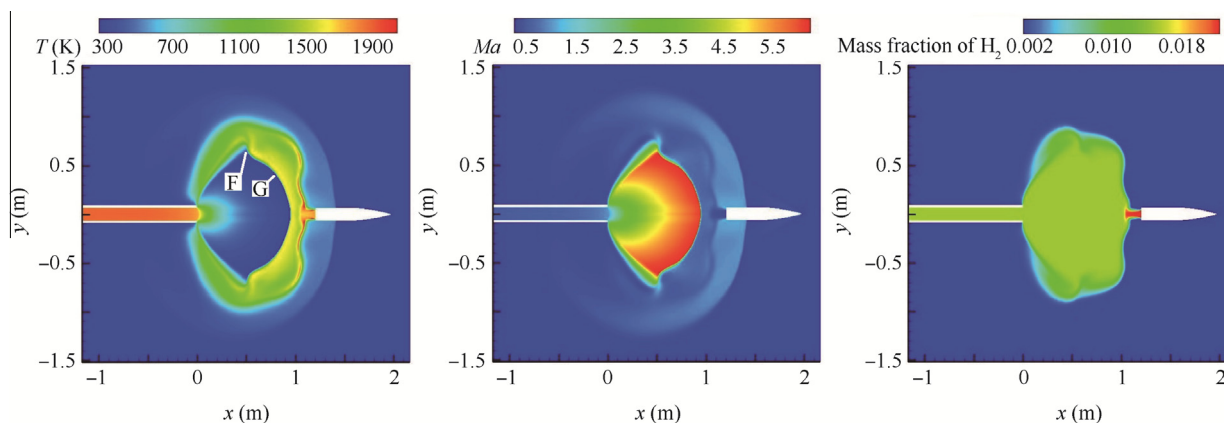
Notes: F—Triple point; G—Mach disk

Fig. 9 Contours of temperature, Mach number and mass fraction of H_2 at t = 1.5 ms.

Fig. 10 Contours of temperature, Mach number and mass fraction of H_2 at t = 2.5 ms.

secondary combustion weakening gradually is that both the concentration of combustible gas (including the CO and H_2) in the propellant gas and pressure near the contact surface gradually decrease with the propagation of the propellant gas.

With the continuous motion of gun-launched missile, as shown in Figs. 11 and 12 at t = 3.5–4.5 ms, the gun-launched

missile has moved through the blast wave and goes to free-flight stage. The flow field around the gun-launched missile can be approximately treated as a steady state. However, the rocket gas injected reversely from the bottom of gun-launched missile interacts with the blast wave and leads to the boundary shape of rocket gas change. In addition, the jet flow field
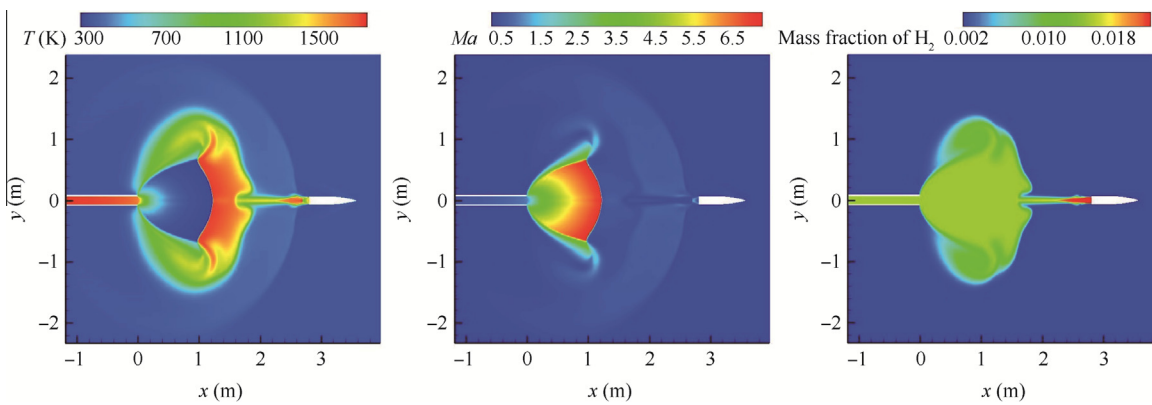
Fig. 11 Contours of temperature, Mach number and mass fraction of H$_2$ at $t = 3.5$ ms.
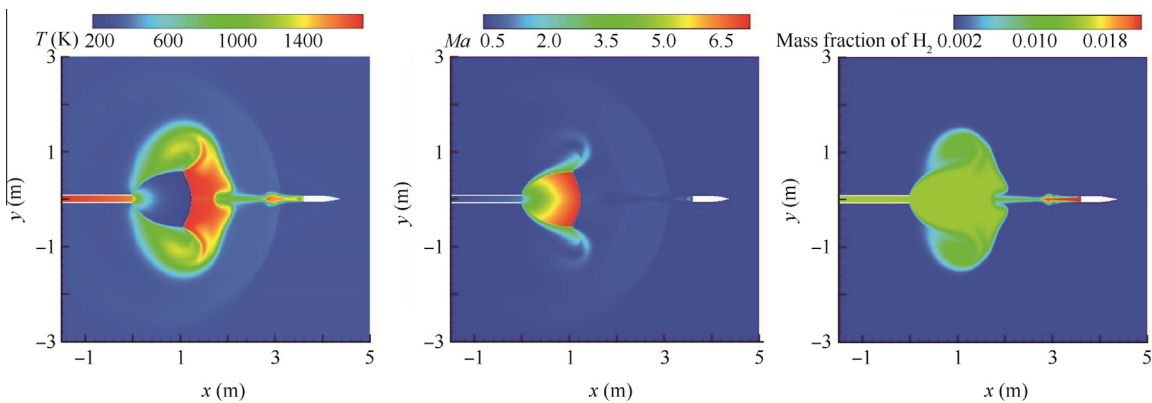

Fig. 12 Contours of temperature, Mach number and mass fraction of H$_2$ at $t = 4.5$ ms.

begins to fully develop: the triple point and incident shock gradually converge toward the central axis and the diameter of the Mach disk gradually decreases.

5.2. Base flow filed of gun-launched missile

Fig. 13 shows the velocity distribution along the central axis between the muzzle and the bottom of missile at different
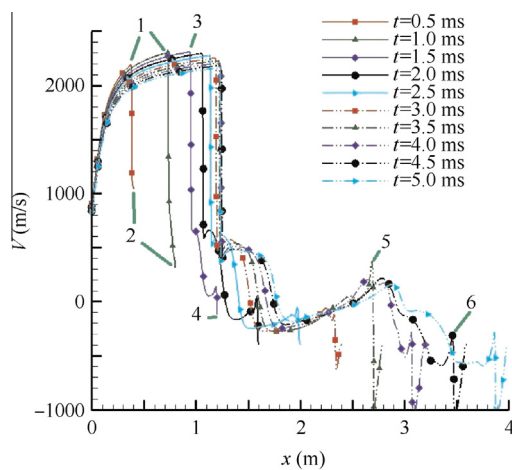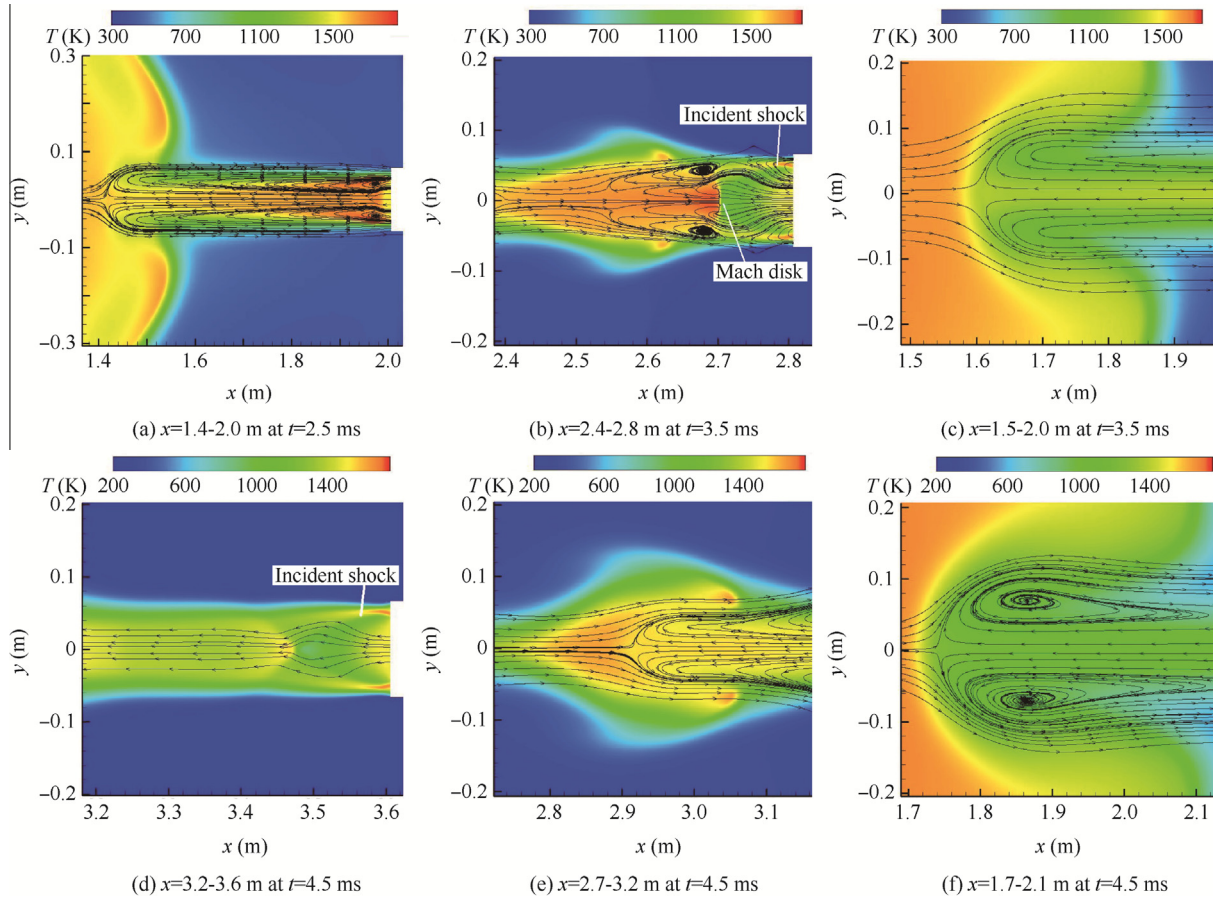

Fig. 13 Velocity distribution along center axis between muzzle and bottom of missile.

time instants. From the curve of velocity distribution at $t = 0.5$ ms and $t = 1.0$ ms, there exists a position "1", where the velocity sharply drops. Because the Mach disk is not completely formed at this time, the position "1" is produced by the base shock. It can also be seen that the velocity of the gas near center axis of missile bottom "2" is still positive, meaning that the rocket gas hardly rushes out of the missile because the flow filed of the missile bottom is in high pressure zone.

At $t = 1.5$ ms, the position "3" that the velocity sharply drops in the curve is produced by the Mach disk because the Mach disk is completely formed after the missile bottom moves through Mach disk. It can also be seen that the center axial velocity of gas at the missile bottom "4" is negative and small, indicating that the rocket gas has rushed out of the bottom of missile and then injects reversely into the propellant gas zone.

From the curve of velocity distribution at $t = 2.0$ ms and $t = 2.5$ ms, it can be seen that the trend of the velocity is quite complex, and the velocity of gas along center axis at $x > 1.5$ m is negative. In order to clearly understand the flow field, the local enlargement of Temperature contour and streamline in the flow field at $t = 2.5, 3.5, 4.5$ ms are shown in Fig. 14. According to Fig. 14(a), the rocket gas which is reversely injected interacts with the propellant gas at $x = 1.4$ m. Meanwhile, a recirculation zone is formed by the rocket gas due to the obstacle of propellant gas and its center axis ranges from about $x = 1.4$–2.0 m.

Fig. 14 Local enlargement of temperature contour and streamline.

According to the curve of velocity distribution at $t = 3.5$ ms, the rocket gas interacts with both the propellant gas and the blast wave and the center axial velocity in several positions is zero. As shown in Fig. 14(b), the flow field near the interaction position where the rocket gas interacts with blast wave is quite complex, and the boundary shape of the rocket gas seriously changes. Meanwhile, a Mach disk is formed in the bottom flow field by the rocket gas, leading to a sudden change of the center axial velocity at $x = 2.7$ m in curve "5". Combined with Fig. 14(a), the recirculation zone formed by the rocket gas is gradually pushed by the propellant gas and moves toward the positive x-axial direction in Fig. 14(c). Meanwhile, the radial length of recirculation zone becomes much longer than the one in Fig. 14(a). In addition, from the curve of velocity distribution, the axial range of the recirculation zone is about $x = 1.6$–2.4 m.

The trend of the velocity distribution at $t = 4.5$ ms is nearly in accordance with the counterpart at $t = 3.5$ ms. As shown in Fig. 14(d), when the bottom of the missile is away from the muzzle blast wave, Mach disk formed by the rocket gas disappears. The upper and lower incident shock formed by the rocket gas intersects along the center axis at about $x = 3.4$ m, leading to the sudden change of the velocity "6". Compared with Fig. 14(a) and Fig. 14(c), the recirculation zone formed by the rocket gas continuously moves toward

the positive x-axial direction in Fig. 14(f), while its axial length becomes gradually shorter than the one at $t = 2.5$ ms and 3.5 ms. From the center axial velocity distribution and the streamline distribution, it can be seen that the recirculation zone becomes complete, independent and closed at this time. The axial range of the recirculation zone is about $x = 1.7$–2.4 m.

6. Conclusions

The development process and flow field structure of muzzle flows including a gun-launched missile are analyzed in detail. From the discussion in the above sections, the numerical investigation can be summarized as follows.

(1) The propellant gas flows, the initial environmental ambient air flows and the moving missile mutually couple and interact. A complete structure of flow field is formed at the launching stages, including the blast wave, base shock, reflected shock, incident shock, shear layer, primary vortex ring and triple point. There exists a high-temperature zone near the contact surface (between the propellant gas and the external air), which results from the secondary combustion of the CO/H_2 in the propellant gas with the O_2 in the external air.

(2) With the continuous motion of gun-launched missile, the recirculation zone formed by the rocket gas is gradually pushed by the propellant gas and moves toward the positive x-axial direction, and the radial length of recirculation zone become much longer. A Mach disk is formed in the bottom flow field by the rocket gas at $t = 3.5$ ms but it disappears at $t = 4.5$ ms.

Acknowledgments

References

1. Guo QY, Jiang Y, Guo LQ. Numerical investigation of aerodynamic characteristic for gun-launched missile. *J Beijing Inst Technol* 2011;**31**(7):772–6 [Chinese].
2. Sui X, Wei ZJ, Wang NF, Bi SH. Analysis of grain intensity in artillery missile motor during launching. *J Ballist* 2009;**21**(2):19–22 [Chinese].
3. Sui X, Wei ZJ, Wang NF, Bi SH. Analysis of effect of the pad material on stress in the grain during launching artillery missile. *Acta Armamentarii* 2009;**30**(6):709–14 [Chinese].
4. Schmidt EM, Shear D. Optical measurements of muzzle blast. *AIAA J* 1975;**13**(8):1086–91.
5. Fansler KS, Schmidt EM. Trajectory perturbations of asymmetric fin-stabilized projectiles caused by muzzle blast. *J Spacecraft Rockets* 1978;**15**(1):62–5.
6. Wang JCT, Widhopf GF. Numerical simulation of blast flow fields using a high resolution TVD finite volume scheme. *Comput Fluids* 1990;**18**(1):103–37.
7. Klingenberg G. Gun muzzle blast and flash. *Propell Explos Pyrot* 1989;**14**(2):57–68.
8. Cler DL. CFD application to gun muzzle blast a validation case study. 2003. Report No.: AIAA-2003-1142.
9. Jiang ZL, Takayama K. Shocked flows induced by supersonic projectiles moving in tubes. *Comput Fluids* 2004;**33**(7):956–66.
10. Cayzac R, Carette E, De Roquefort TA, Renard FX, Roux D, Balbo P, et al. Computational fluid dynamics and experimental validation of the direct coupling between interior, intermediate and exterior ballistics using the Euler equations. *J Appl Mech Trans ASME* 2011;**78**: 061006-1/061006-17.
11. Batina JT. Unsteady Euler algorithm with unstructured dynamic mesh for complex-aircraft aerodynamic analysis. *AIAA J* 1991;**29**(3):327–33.
12. Yen GW, Baysal O. Dynamic-overlapped-grid simulation of aerodynamically determined relative motion. 1993. Report No.: AIAA-1993-3018.
13. Kim JW, Park SH, Yu YH. Euler and Navier-Stokes simulations of helicopter rotor blade in forward flight using an overlapped grid solver. 2009. Report No.: AIAA-2009-4268.
14. Fumito T, Matsuo A. Numerical investigation of sabot separation process in a ballistic range using moving overlapped grid method. 2013. Report No.: AIAA-2013-0496.
15. Zhang HX, Chen JQ, Gao SC. Numerical simulation of supersonic non-equilibrium flows for H_2/O_2 combustion. *J Astronaut* 1994;**14**(2):14–22 [Chinese].
16. Barth TJ, Jespersen DC. The design and application of upwind schemes on unstructured meshes. 1989. Report No.: AIAA-1989-0366.
17. Kim KH, Kim C, Rho OH. Methods for the accurate computations of hypersonic flows: I. AUSMPW+ scheme. *J Comput Phys* 2001;**174**(1):38–80.
18. Gibeling HJ, Nietubicz CJ. Navier-Stokes computations for a reacting, M864 base bleed projectile. 1993. Report No.: AIAA-1993-0504.
19. Zhuo CF, Wu XS, Feng F. Numerical simulation of supersonic non-equilibrium flows using kinetic scheme. *J Ballist* 2013;**25**(3): 88–94 [Chinese].
20. Lee KR, Park JH, Kim KH. High-order interpolation method for overset grid based on finite volume method. *AIAA J* 2011;**49**(7): 1387–98.
21. Evans JS, Schexnayder CJ. Influence of chemical kinetics and unmixedness on burning in supersonic hydrogen flames. *AIAA J* 1980;**18**(2):188–93.
22. Lehr HF. Experiments on shock-induced combustion. *Acta Astronautica* 1972;**17**:589–97.
23. Soetrisno M, Imlay ST. Simulation of the flow field of a ram accelerator. 1991. Report No.: AIAA-1991-1915.
24. Yungster S, Eberhardt S, Bruckner AP. Numerical simulation of hypervelocity projectiles in detonable gases. *AIAA J* 1991;**29**(2): 187–99.

Zhuo Changfei is a Ph.D. student at Nanjing University of Science and Technology. His area of research includes computational fluid dynamics and the aerodynamics of missiles.

Feng Feng received the Ph.D. degree at Nanjing University of Science and Technology in 2010, and then became a teacher there. His main research interests are computational fluid dynamics, the aerodynamics of missiles and propulsion technology.

Wu Xiaosong is a professor and Ph.D. supervisor at Nanjing University of Science and Technology. His current research interests are computational fluid dynamics and propulsion technology.